LAWRENCE
LIVERMORE
NATIONAL
LABORATORY

LLNL-CONF-643521

Performance of CID camera X-ray imagers at NIF in a harsh neutron environment

N. E. Palmer, M. B. Schneider, P. M. Bell, K. Piston, J. Moody, D. James, R. Ness, M. Haugh, J. Lee, E. Romano

September 6, 2013

SPIE Conference
San Diego, CA, United States
August 25, 2013 through August 29, 2013

Disclaimer

Performance of CID camera X-ray imagers at NIF in a harsh neutron environment

Nathan E. Palmer*[a], Marilyn B. Schneider[a], Perry M. Bell[a], Ken W. Piston[a], James D. Moody[a], D. Lynn James[a], Ron A. Ness[a], Michael J. Haugh[b], Joshua J. Lee[b], Edward D. Romano[b]
[a]Lawrence Livermore National Laboratory, 7000 East Ave., Livermore, California 94550
[b]National Security Technologies, LLC, 161 S. Vasco Rd., Suite A, Livermore, California 94551

ABSTRACT

Charge-injection devices (CIDs) are solid-state 2D imaging sensors similar to CCDs, but their distinct architecture makes CIDs more resistant to ionizing radiation.[1–3] CID cameras have been used extensively for X-ray imaging at the OMEGA Laser Facility[4,5] with neutron fluences at the sensor approaching 10^9 n/cm^2 (DT, 14 MeV). A CID Camera X-ray Imager (CCXI) system has been designed and implemented at NIF that can be used as a rad-hard electronic-readout alternative for time-integrated X-ray imaging. This paper describes the design and implementation of the system, calibration of the sensor for X-rays in the 3 – 14 keV energy range, and preliminary data acquired on NIF shots over a range of neutron yields. The upper limit of neutron fluence at which CCXI can acquire useable images is ~ 10^8 n/cm^2 and there are noise problems that need further improvement, but the sensor has proven to be very robust in surviving high yield shots (~ 10^{14} DT neutrons) with minimal damage.

Keywords: CID, charge-injection device, X-ray imaging, CCXI, neutron fluence, radiation hardness, NIF, National Ignition Facility

1. INTRODUCTION

For inertial confinement fusion (ICF) target implosions at the National Ignition Facility (NIF), the primary diagnostics for X-ray imaging are high-speed framing cameras and streak cameras such as GXD[6] and DISC.[7] These instruments provide time-resolved measurements of key ICF performance metrics such as implosion velocity and hot spot shape/symmetry.[8] There is also a suite of time-integrated X-ray imaging diagnostics that, while typically secondary in importance, provide valuable data for many applications. These include confirming the alignment of the diagnostic positioners, measuring the time-integrated hot spot shape, measuring the clear aperture of the laser entrance hole, confirming the pointing of the laser beams on the target, measuring the symmetry of the X-ray emission from the two ends of the hohlraum, or serving as the detector for an X-ray spectrometer.

Due to the harsh neutron environment at NIF (neutron fluences ~ 10^9 n/cm^2, routinely exceeding the saturation and damage levels for CCD cameras), most of the time-integrated X-ray images at NIF are currently recorded on image plate or film. For certain applications at NIF, rad-hard charge-injection device (CID) cameras can replace image plates, leveraging the significant advantages of electronic readout. These include having data available within seconds after the shot instead of hours to days for image plate or film, much more efficient operation since no access to the target chamber or diagnostics is required to retrieve the data, and enhanced safety because technicians avoid radiation dose they would otherwise receive going in to retrieve media.

This paper describes the design and implementation of a CID Camera X-ray Imager (CCXI) system for Diagnostic Instrument Manipulator (DIM)-based diagnostics at NIF. We present sensor calibration results for X-rays in the 3 – 14 keV energy range, as well as preliminary data from NIF shots in which the capability and radiation hardness of the CCXI system were evaluated.

2. CID IMAGING SENSOR CHARACTERISTICS

The imaging sensor used for this work is the CID4150 from Thermo Scientific, CIDTEC Cameras & Imagers.[1,9] The sensor was selected based on a history of successful use on ICF experiments at the Univ. of Rochester's OMEGA Laser Facility.[4,5]

*palmer36@llnl.gov; phone: 1 925 423-2558; www.llnl.gov

2.1 The CID4150 sensor

The front and back sides of the CID imager module are shown in Figure 1. This highly compact device (31 × 23 × 5 mm) was originally developed for dental X-ray imaging, and is an 800 × 600 array of 38.5 µm square pixels. The pixels have a large full well capacity of > 10^6 electron-hole pairs.

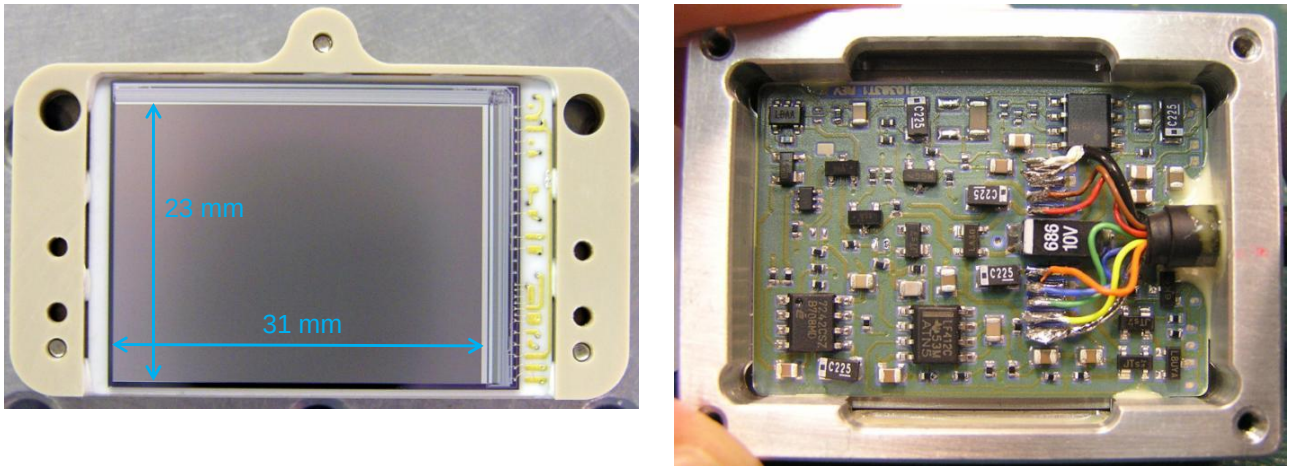

Figure 1. Front- and back-side views of the CID4150 imaging sensor.

In this compact package the CID sensor die is mounted directly on a ceramic circuit board with ancillary readout electronics on the back side. There is no thermoelectric cooler, so the sensor operates at room temperature in vacuum or in air. The dark current is thus quite high, and this (along with some limitations of the readout electronics) limits the maximum integration time to less than ~ 5 sec. This is not a problem at NIF, where the signal is very bright and is produced in a nanoseconds burst, so a convenient integration time of 100 ms was implemented. However, the limited integration time did present a problem during sensor calibration (described in Section 4 below) using DC sources with limited X-ray flux, which necessitated acquiring a large number of replicate images to improve the signal-to-noise ratio.

For this application the sensor is uncoated and detects X-rays directly as they interact with the active epitaxial Si layer in the pixels. The X-ray energy sensitivity range for the uncoated sensor is 1 – 15 keV. Phosphor coatings are available to extend the X-ray sensitivity up to ~ 100 keV, and the phosphor thickness can be tailored to a specific energy range of interest.

Readout of the pixels is progressive at 500 kHz, so it takes ≈ 1 sec. to read out the 800 × 600 image. The nondestructive readout capability of CIDs was not implemented for this camera. The readout is via an analog video signal, 1.0 Vpp, which is transmitted via coaxial cable to a remote 16-bit digitizer. The dynamic range estimated by the vendor is > 1000:1, and the limiting resolution is 10 LP/mm.

2.2 CID radiation hardness

There are several distinctive features of CIDs that make them more resistant to ionizing radiation.[1–3] These CID cameras are fabricated using a high-resistivity P-channel process and have a rated lifetime dosage of at least 300 krad(Si) at 60 – 90 keV. That is ~ 20× higher than typical N-channel CCD cameras which cease to function after 10 – 20 krad(Si). Other CID cameras are available that have lifetime dosage > 3 Mrad(Si).[10]

In addition, unlike CCDs which read out by transferring charge from pixel to pixel across entire columns and are thus highly sensitive to charge transfer efficiency (which degrades under radiation), CIDs read out by transferring charge once from one photogate to another within the same pixel, and are thus insensitive to charge transfer efficiency. The fact that CIDs do not transfer charge outside the pixel also makes them inherently anti-blooming, in that excess charge within a pixel diffuses into the substrate rather than spilling over into neighboring pixels. The pixels of the sensors in this work also have a large full well capacity (> 10^6 electron-hole pairs) which extends the range of exposure they can handle before saturating, and the discrete analog components used with these imagers for signal amplification and readout are more rad-hard (less prone to upsets) than high-density digital circuits.

3. CCXI SYSTEM IMPLEMENTATION AT NIF

3.1 CCXI hardware assembly

The CCXI camera head assembly for fielding on DIM-based diagnostics is shown in Figure 2. The assembly consists of two CID camera modules, each having a 25 μm polyimide film over the face of the sensor as a protective cover, and a 3 mm thick tungsten alloy frame that shields the edges of the sensors and protects the on-chip logic. In preliminary CID testing at the COMET laser of the Jupiter Laser Facility,[11] it was found that if X-rays hit the on-chip logic or if the cables were not well shielded against electromagnetic interference (EMI) then it caused "drop-outs", meaning the sensor would not read out a complete image. The small circuit board attached to the feedthrough flange provides EMI filtering for the DC power lines, as well as differential line receivers for the CLOCK and TRIG signals (more about this under Electrical Design below). The video signal (image output) is transmitted via micro coax.; all other signals via Tefzel-jacketed hook-up wire. Since the cameras are used inside the NIF target chamber vacuum, all materials are required to meet stringent requirements for cleanliness and low outgassing.

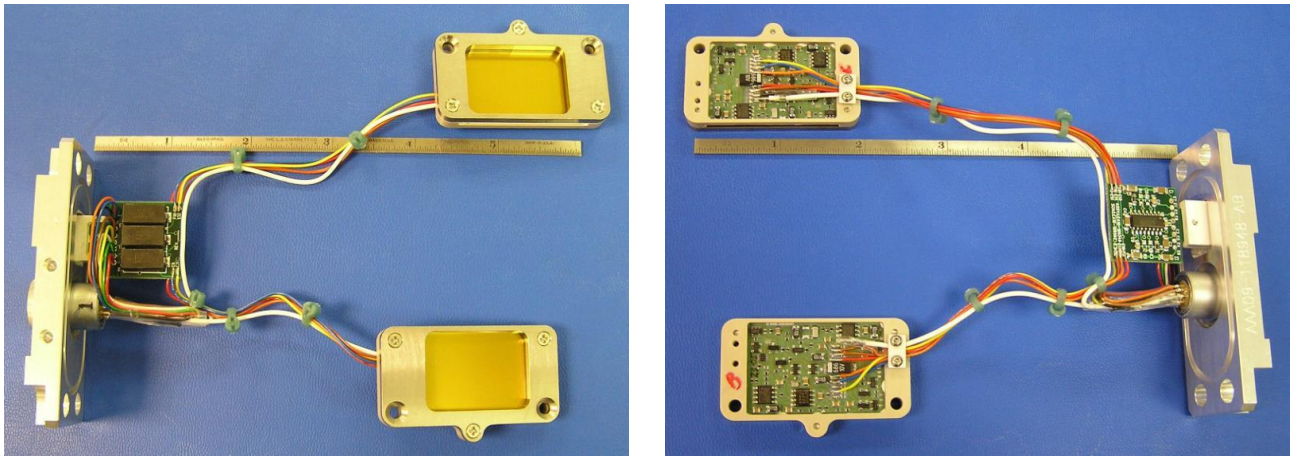

Figure 2. Front- and back-side views of the CCXI camera head assembly built for DIM-based diagnostics at NIF.

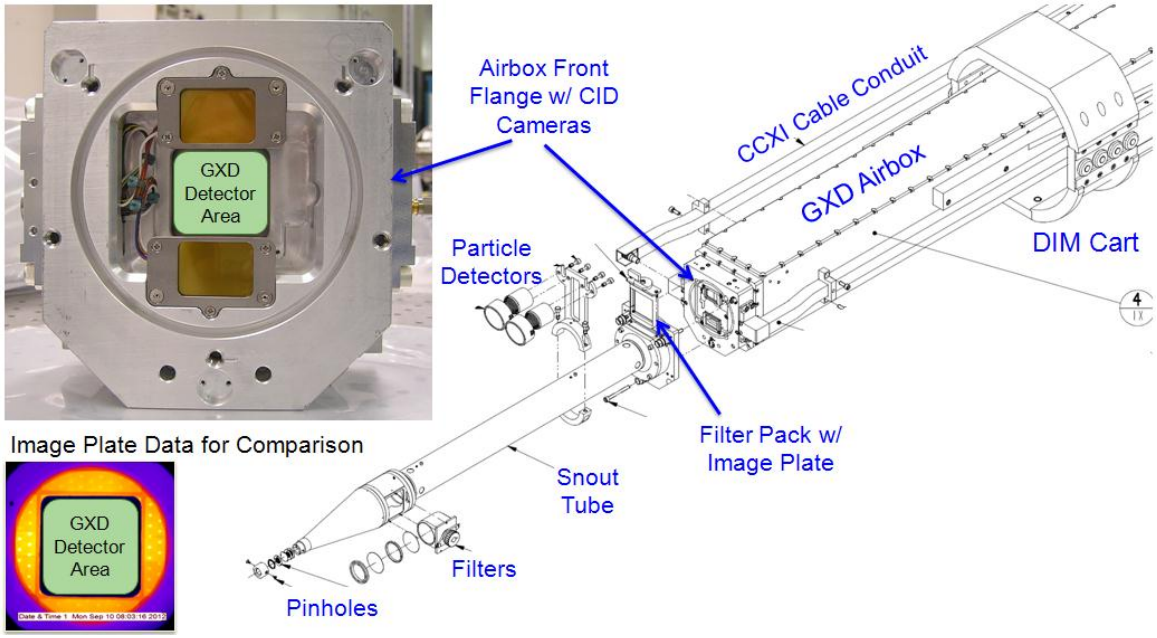

Figure 3. CCXI mounted on a DIM-based diagnostic package (GXD in this example; drawing excerpt from AAA10-106125-AA). The CID cameras sit ~ 125 cm from the target, where neutron fluence can exceed 10^9 n/cm^2.

Figure 3 shows how the CCXI camera head assembly is mounted on a DIM-based diagnostic. The CID cameras are installed in small pockets on the front of the airbox front flange, with the camera modules slightly recessed below the surface of the flange. The CID cameras are positioned directly above and below the line of sight of the main diagnostic (GXD in this example), where they can record images from peripheral pinholes. For comparison, the inset at the lower left of Figure 3 shows an example of how peripheral pinhole images are currently recorded on image plate — a function that CCXI can replace, at least for the top and bottom lines of sight. Depending on the snout configuration, the CID cameras on a DIM-based diagnostic typically sit ~ 125 cm from the target, where neutron fluence can exceed 10^9 n/cm^2.

3.2 Electrical design

A schematic of the CCXI electrical design is shown in Figure 4. The CCXI electronics and controls are completely independent of the main DIM-based diagnostic (such as GXD) on which it is installed. The inputs to the CCXI camera head are DC power (+5V, +8V, and -7.5V from the Agilent N6700B power supply), a 1 MHz clock signal from the ATS660 digitizer card in the data acquisition computer, and trigger pulses from the DG645 delay generator. The CCXI Interface Chassis in the Diagnostic Mezzanine is the hub for sending these inputs to the CCXI head via the infrastructure and DIM cables. The outputs from the CCXI head are two analog video signals (one for each CID camera) transmitted to the 16-bit digitizer via coaxial cables. No other utilities (such as cooling water) are needed for CCXI, since the cameras operate at room temperature.

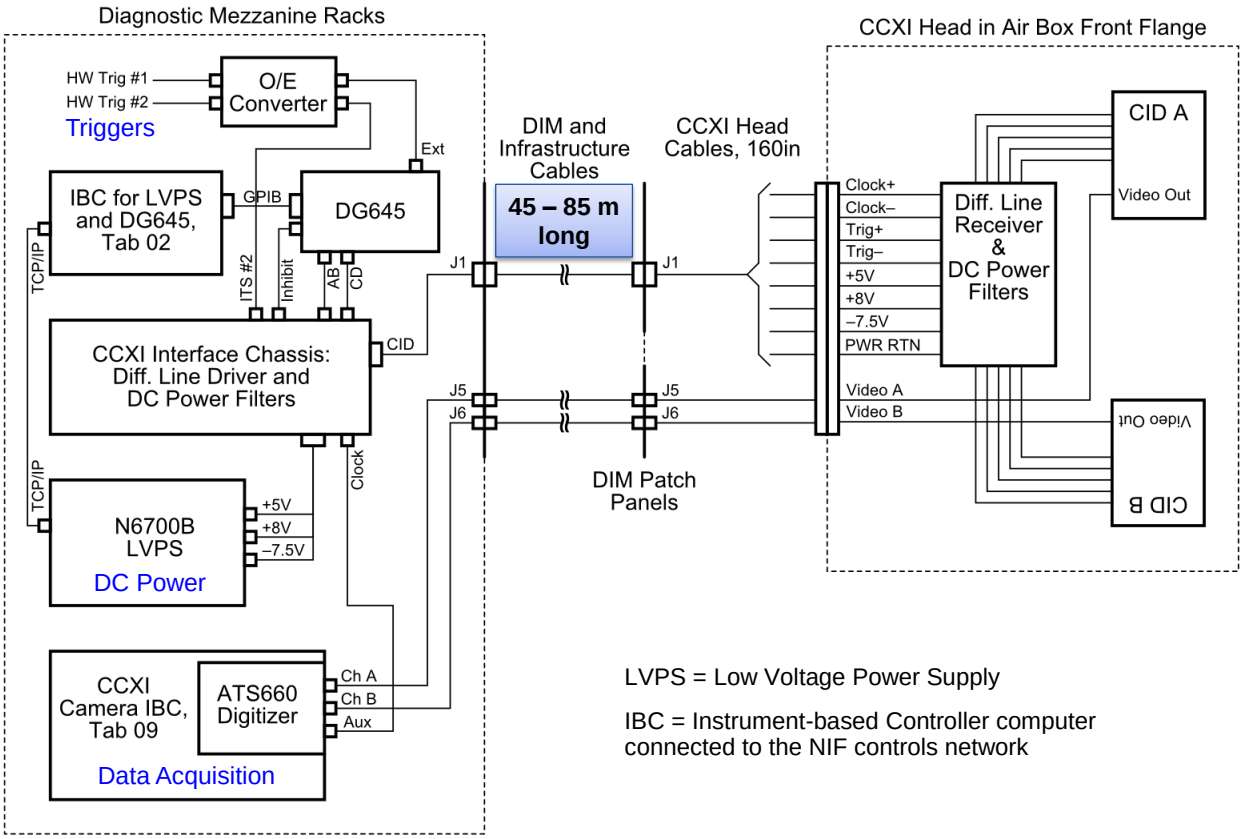

Figure 4. Schematic of CCXI electrical design. One of the big challenges is to transmit these low-voltage analog signals over 45 – 85 m long cables in a noisy EMI/EMP environment.

When CCXI was designed and deployed there were a limited number of coaxial signal cables available in the DIM and infrastructure cable plant — only 1 coax. per CID — so these were used for the Video Out (image data) signals. This meant the CLOCK and TRIG signals had to be transmitted over long twisted-pair cables, which necessitated using a differential line driver/receiver combination. The differential line drivers are in the CCXI Interface Chassis in the Diagnostic Mezzanine, and the receivers are on the small circuit board in the CCXI head. This solution works but also exacerbates one of the main noise sources for these CID cameras, which is clock noise bleed-over into the readout amplifiers.

Recommended future improvements include upgrading the cable plant to transmit the CLOCK and TRIG signals via coax. and eliminate the differential line drivers/receivers. Signal-to-noise could be further improved by fine-tuning the delay of the CLOCK signal to get optimal analog-to-digital samples at points in the readout waveform where noise is lowest. Finally, good grounding and EMI shielding are essential to minimize noise pickup on these low-voltage analog signals over long cables in the EMI/EMP environment of the NIF, and the EMI shielding for CCXI could be further improved.

3.3 CCXI system timing

The CID cameras used for CCXI have operating characteristics that presented some challenges for the NIF timing system. Experience at OMEGA plus preliminary testing at LLNL confirmed that these cameras perform best — have lower readout noise and more stable "black level" (reference pixel level) — if the camera is triggered and read out several times in a row prior to acquiring the background and shot data images. Also, to achieve the highest quality background image subtraction for these room temperature cameras with large drift, the background image must be acquired less than a few seconds before the shot. Thus, a system had to be devised to send a train of trigger pulses to the cameras in the final seconds before the shot, with the final pulse synchronized to the laser shot.

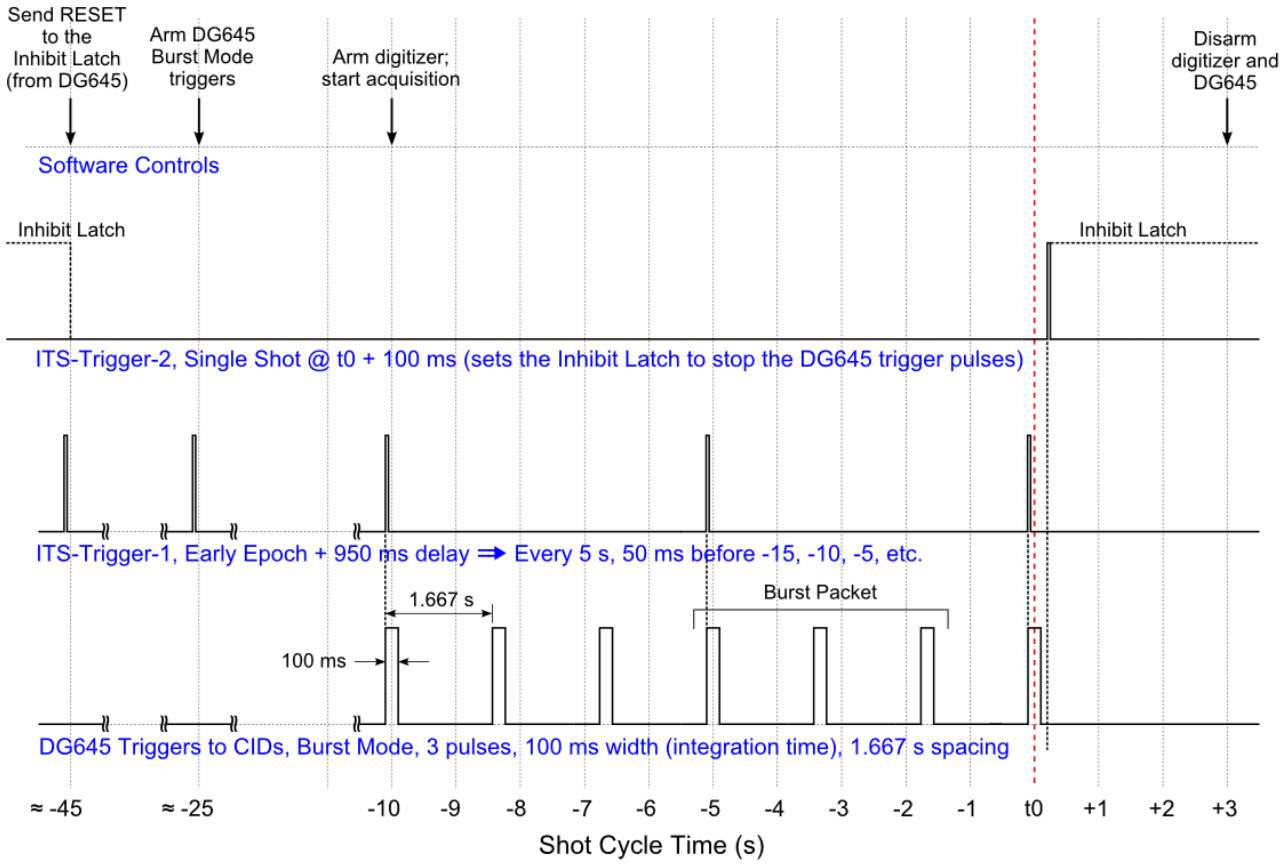

Figure 5. Diagram of CCXI system triggers and timing for a shot countdown at NIF. The trigger pulses to the CID cameras are shown on the bottom row — a train of 100 ms wide pulses, with a pulse every 1.667 s. The cameras integrate and readout an image for each trigger pulse, but only the last three images are archived — the shot image and two preshot images for background subtraction.

The timing solution that was implemented for CCXI at NIF is illustrated in Figure 5. The sequence of events in the countdown to a shot is as follows. At t – 45 s, NIF control software causes a RESET signal to be sent to the Inhibit Latch in the CCXI Interface Chassis (so that trigger pulses are not inhibited). At t – 25 s, the DG645 is armed in a burst mode, such that it starts sending bursts of trigger pulses to the CID cameras, synchronized to (externally triggered by) the hardware trigger ITS-Trigger-1. As shown on the bottom row of Figure 5, the trigger pulses to the cameras are 100 ms wide (the width of the trigger pulse sets the length of the integration time) with a pulse every 1.667 s. The use of the

Early Epoch (a set of triggers 1 sec. ahead of the other hardware triggers) was key to be able to trigger the CID cameras sufficiently early (50 ms prior to the shot for the final pulse). The cameras start integrating and reading out an image for each trigger pulse (readout takes ≈ 1 sec.), but the data doesn't start being saved until t – 10 s when the digitizer is armed. The digitizer triggers on the leading edge of the video signal (the beginning of each readout) and starts saving the readout waveforms into a circular memory buffer large enough to hold around 10 images. The digitizer continues acquiring image data into the buffer indefinitely until it is disarmed (after the shot) by a software command, and is not directly aware of when the shot occurs. This flexibility was necessary (instead of acquiring a fixed number of images or using a software command to end the acquistion) because there is so much variability in the execution of complex commands during the shot countdown that the synchronization between the NIF control software clock and the timing system hardware clock can sometimes slip by 5 sec. (to the following pulse in the Early and Long Epochs). Hence, a second hardware trigger (ITS-Trigger-2) was needed to set the Inhibit Latch at t + 100 ms and prevent the DG645 from sending any more trigger pulses after the shot. This ensures that the shot data is always the last image saved. At t + 3 s, the digitizer is disarmed, and the shot image and the two preceding preshot images are processed from the memory buffer and archived.

4. CID CAMERA CALIBRATION

To prepare for quantitative measurements with CCXI at NIF, a set of calibrations was undertaken using the X-ray sources and calibration facilities at National Security Technologies, LLC (NSTec), Livermore Operations.[12] After overcoming some challenges described below, the CID cameras were characterized for responsivity, resolution, and linearity and saturation.

4.1 CID calibration challenges

Compared to scientific cameras, there were significant challenges to calibrate these CIDs which were designed for qualitative imaging in industrial applications such as dental X-rays or material inspection. As previously described, the integration time for these cameras is limited to ~ < 5 sec. due to high dark current (room temperature operation) and limitations of the readout electronics. (For certain cameras tested, the readout after integration longer than ~ 5 sec. was not reliable and would sometimes drop out, producing only a partial image even if the image did not saturate.) Due to the combination of short integration time plus limited flux from the available X-ray sources plus low responsivity of the CIDs, the photon statistics in individual images were overwhelmed by other noise sources (readout and pattern noise, including clock noise bleed-over as described above). This meant that the photon transfer statistical methods of Janesick[13] could not be used to characterize the gain and the linear range of these cameras, and that a large number of (~50) background-subtracted images would be required to collect enough photons to improve the signal-to-noise. The other limitation is that due to the large drift in background noise over time for these room-temperature cameras, the background images must be acquired within seconds of the X-ray images in order to achieve good background subtraction.

To address these challenges, new data acquisition software was created by NIF Target Diagnostics Software developers to enable acquiring a large batch of images (up to 100 frames from each CID camera, limited at the time only by the available memory on the acquisition computer). In addition, a system was devised using two interconnected delay generators to send a series of up to 100 trigger pulses to the cameras (with up to 3 sec. integration for each pulse) while only triggering the shutter on the X-ray source for every other pulse. In this way, a background image was acquired immediately after each X-ray image, and a total of up to 50 X-ray/background image pairs could be collected in a single run.

4.2 Responsivity vs. X-ray energy

The CID camera responsivity (mean counts / pixel / incident photon) was measured at each energy from the average of 50 background-subtracted images as described above, with X-ray energies of 3 – 7.7 keV using the Manson source, and 8 – 14 keV using the HEX source.[12] The results are shown in Figure 6, in which the measured values for three different CID cameras are compared to a simple model based on the transmission of a Si dead layer of specified thickness and the absorption of a Si active layer of specified thickness. Model 1 uses our initial estimates of a 1 μm dead layer, 7 μm active layer, and κ = gain = 56 electron-hole (e-h) pairs per count, and is not a good fit to the measured values. In Model 2 the parameters were adjusted for a better fit — 2.2 μm dead layer, 6.7 μm active layer, and scale factor of 0.75. The 0.75 scale factor is probably mainly due to error in our initial estimate of κ, which was derived from estimates for the pixel full well value (1.4×10^6 e-h pairs) and the maximum number of counts in strongly saturated pixels (≈ 25,000).

The use of saturated pixels led to underestimating the gain, which is probably closer to 56 / 0.75 ≈ 75 e-h pairs per count over the linear (unsaturated) range of response. Follow-up testing with visible light is needed to get a better measurement of κ. Other possible factors that could help explain the 0.75 scale factor are a smaller-than-expected effective area for the pixels or charge collection efficiency of less than 100% for detected photons. The bottom curve in Figure 6 includes the transmission through the 25 µm polyimide cover over the face of the sensors, and represents the responsivity of the camera assembly as used at NIF (not including any additional filters placed in front of the cameras).

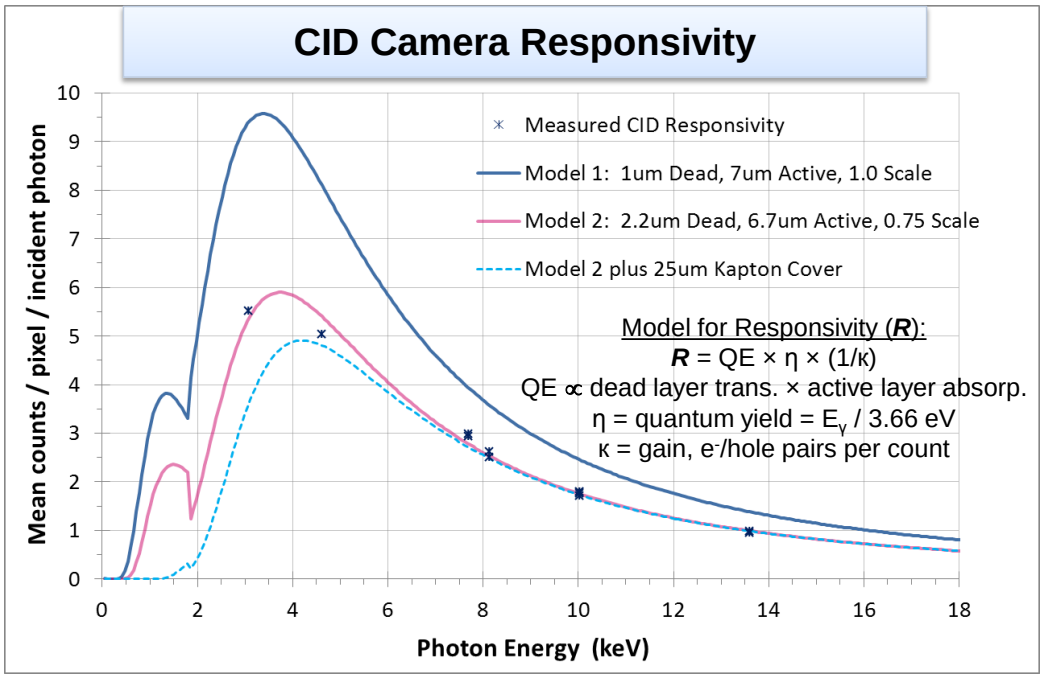

Figure 6. CID camera responsivity measurements for X-rays from 3 to 14 keV, with simple models for comparison. In Model 2 the parameters were adjusted to fit the measured values. The bottom curve (small dashes) includes the transmission through the 25 µm polyimide cover over the face of the sensors, and represents the responsivity of the camera assembly as used at NIF (not including any additional filters placed in front of the cameras).

4.3 Resolution

Figure 7 shows an image that was taken with a resolution mask over the CID camera. The image is actually an average of 50 background-subtracted images, 1 sec. exposures, with 4.6 keV X-ray illumination from the Manson source (Ti anode, no filter). The dark outer edges are the shadow of the thick tungsten frame on the camera module. The numbers on the mask indicate line pairs per mm (LP/mm). The limiting resolution — the finest line pattern that the camera can resolve — is defined as the line spacing for which the modulation transfer function (MTF; i.e., the contrast between adjacent dark and light bands) is down to 50% compared to the fully resolved patterns. For this CID camera, the MTF = 50% at ≈ 10 LP/mm, in good agreement with the vendor's reported value.

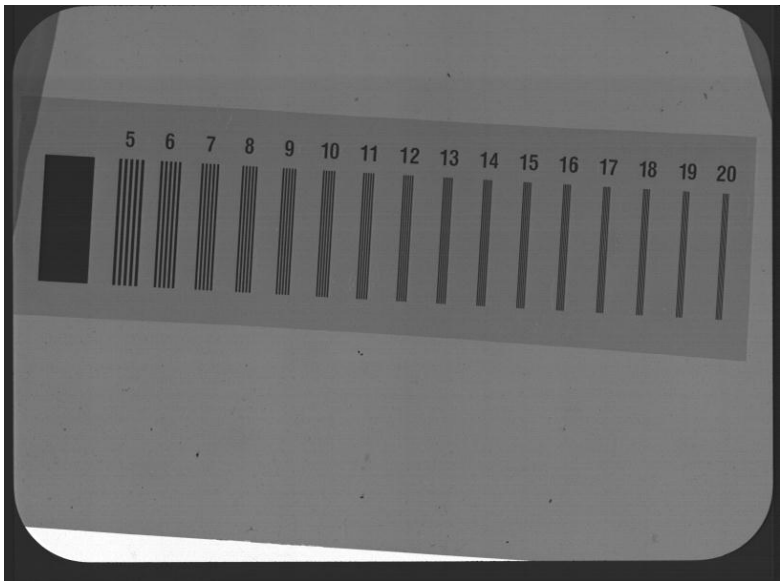

Figure 7. CID camera image with resolution mask. The numbers on the mask indicate line pairs per mm (LP/mm). The limiting resolution (the finest line pattern that the camera can resolve) is approximately 10 LP/mm.

4.4 Linearity and saturation

Since the X-ray sources at NSTec could not produce enough counts in a single CID camera image to measure the full linear range, a test with a variable visible light source was used instead. In the course of this testing, a nonphysical saturation behavior was discovered. For flat-field illumination (uniform illumination over the entire sensor), the output is linear up to ≈ 16,000 counts/pixel (≈ 1 V), then the output starts to "oscillate," swinging high and low on every other row, producing a pattern of dark and light bands in the image as shown in Figure 8. Interestingly, if instead of a flat field, the illumination is confined to a small region on the sensor (less than ~100 pixels wide) such as a pinhole image of an ICF target implosion, then the saturation level appears to be somewhat higher: ≈ 20,000 counts/pixel or ≈ 1.2 V. This nonphysical saturation behavior appears to be a limitation of the integrated readout electronics (rated for 1.0 Vpp) and not of the CID chip itself.

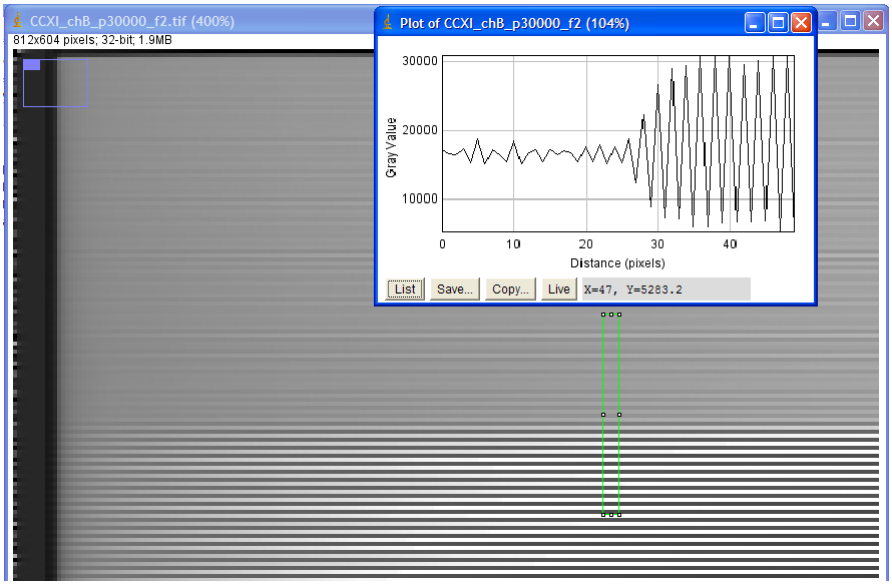

Figure 8. CID camera image (zoomed in to see details of individual rows) showing onset of saturation oscillation with alternating rows of high and low output. The inset (top right) is a vertical lineout for the ROI highlighted in green.

5. CCXI PERFORMANCE AND RADIATION HARDNESS AT NIF

In order to evaluate the performance and radiation hardness of CCXI at NIF, CCXI was fielded on DIM-based diagnostics (GXD and hGXI) in DIM 0-0 (Polar DIM) and DIM 90-78. (CCXI was not commissioned in DIM 90-315 due to shorts in the infrastructure cable.) For these preliminary tests CCXI was a tertiary "ride-along" diagnostic, so the pinholes and filters in the diagnostic snouts were not configured specifically for CCXI with an imaging line of sight. Rather, the CID cameras were exposed to diffuse X-ray illumination coming through the snout, filters, and enclosing hardware. A sample of images thus acquired by CCXI on NIF shots is shown in Figures 9 and 10.

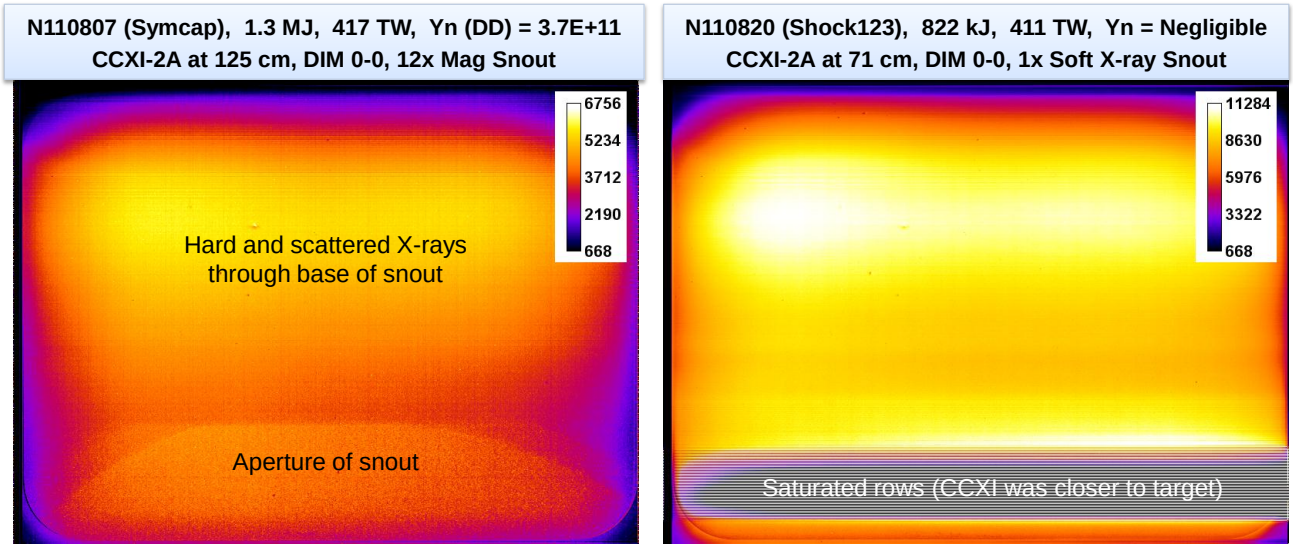

Figure 9. False-color, background-subtracted CCXI images acquired on low-neutron-yield shots with diffuse X-ray illumination coming through the snout, filters, and enclosing hardware. For the image on the right, CCXI was closer to the target (71 cm, vs. 125 cm for the image on the left) so the X-ray flux was more intense and part of the image saturated.

5.1 Noise and dynamic range

The noise floor for CCXI preshot (background) images at NIF was significantly higher (2x – 4x) than the noise in background images from offline testing. This is a consequence of the long cable runs and noisy EMI environment at NIF, and this noise could be reduced by further improvements in the EMI shielding for CCXI. In any case, to quantify the dynamic range for the current implementation, the typical noise (standard deviation of counts) in a 100 × 100 pixel region at the center of a NIF preshot image is ≈ 200 – 400 counts. Given the saturation limits of ≈ 16,000 counts for broad illumination and ≈ 20,000 counts for small spot illumination, the dynamic range is ≈ 40:1 – 80:1 (broad) or ≈ 50:1 – 100:1 (small spot).

The high dark current of these room-temperature sensors also eats away the dynamic range by raising the bias level of the noise floor. Cooling the sensor could dramatically decrease the dark current, but it would also add significant complexity to the design, require new utilities, and sacrifice the compact size of the camera module.

5.2 Neutron fluence saturation limits

CCXI ran on NIF shots with a range of neutron yield (Y_n) from negligible up to 4.5×10^{14} neutrons (DT, 14 MeV), meaning a neutron fluence at the sensor of up to 2.3×10^9 n/cm^2 on a single shot. As shown by the sample image in Figure 10, CCXI was able to obtain usable images on shots with n-fluence of 2.4×10^7 and 4.3×10^7 n/cm^2 at the sensor ($Y_n = 4.27 \times 10^{12}$ and 8.5×10^{12}). For shots with n-fluence greater than 8.8×10^8 n/cm^2 ($Y_n > 1.7 \times 10^{14}$), the CCXI images saturated. The exact neutron saturation limit for CCXI was not measured because none of the shots during this evaluation had Y_n in the ~ 10^{13} range. However, the results just mentioned are consistent with results at OMEGA[4] and consistent with calculations in Table 1 below of CID camera saturation compared to image plate. It is therefore estimated that CCXI can acquire usable images for neutron fluence up to ~ 10^8 n/cm^2 (Y_n ~ 5×10^{13} neutrons with the CIDs at 125 cm from the target). In comparison, image plate can acquire usable data for up to an order of magnitude higher n-fluence (~ 3×10^9 n/cm^2).

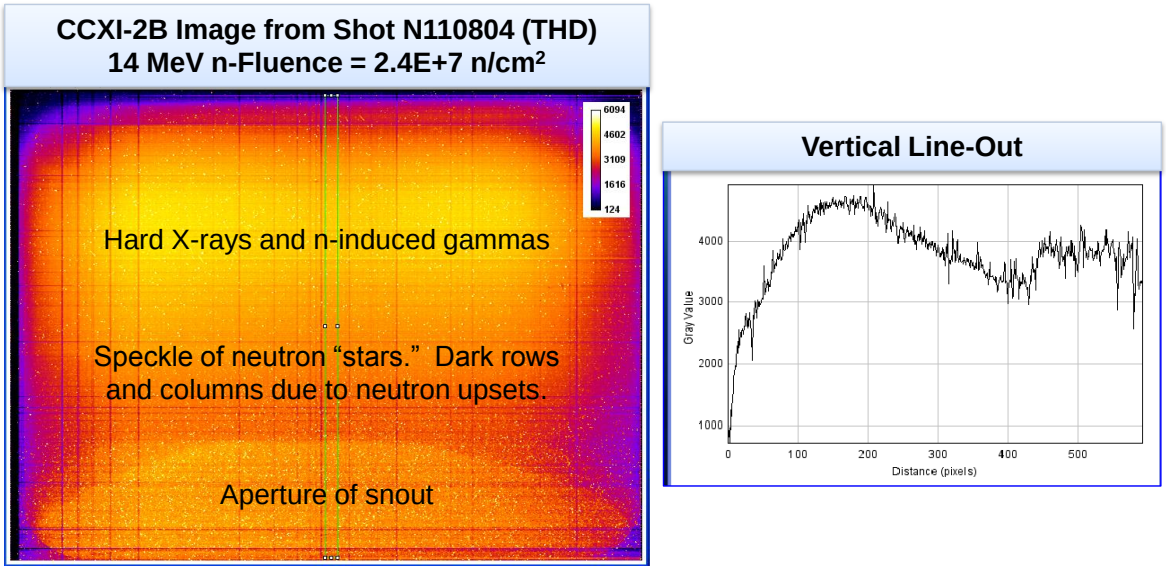

Figure 10. False-color, background-subtracted CCXI image showing the effects of neutron fluence. Neutrons produce bright single-pixel events referred to as "stars" and cause upsets that produce some dark rows and columns. Neutron-induced radiation also raises the overall background level of the image, reducing dynamic range.

Table 1. Estimated saturation limits for CIDs vs. type SR image plate. (Calculation by N. Izumi, LLNL, 15 August 2011)

Detector:	BAS-SR Image Plate	CID4150 for CCXI
Pixel size	25um	38.5um
Material	BaFBr(Eu)	Si
Protection layer	PET ~7um	SiO2 ~1um
Sensitive layer	39 mg/cm2	1.63 mg/cm2
Energy absorption @ 10keV	97.5%	5.2%
Saturation limit	1.265E+5 PSL/mm2	1E+6 electron/pix
Signal saturation (absorbed)	**63 erg/cm2**	**0.40 erg/cm2**
14 MeV Neutron sensitivity	~1.3 keV/inc. n	130 eV/ inc. n
n-fluence equiv. to saturation	3E+10 n/cm2	1.9E+9 n/cm2
Practical n-fluence limit	3E+9 n/cm2	3E+8 n/cm2**
Practical Yn limit at 125 cm	**5.9E+14**	**5.9E+13**

** Practical neutron fluence limit for CID4150 reported by Marshall, DeHaas, and Glebov[4]

5.3 X-ray damage

During many of the evaluation shots at NIF that did not have filtering designed specifically for CCXI, the CID cameras were overexposed to X-rays, resulting in some burn-in damage as shown by the images in Figure 11. The image on the left is a dark image (background-only image with no light) for a pristine new camera (CCXI-2B), before being fielded at NIF. The image on the right is a dark image for the same camera after exposure to multiple shots at NIF with negligible neutron yield. The X-ray damage is evident by the burned-in pattern of the shadow of the tungsten frame around the edge of the sensor. The exposed pixels in the center of the camera now have higher dark current than the edge pixels that were shielded. The standard deviation of dark current counts in the central region increased by ~ 1.7x, and the mean increased by 558 counts. Repeated overexposure to X-rays can increase the dark current to the point that the cameras become unusable and need to be replaced. However, X-ray damage can be minimized with appropriate filtering in front of the cameras to prevent overexposure.

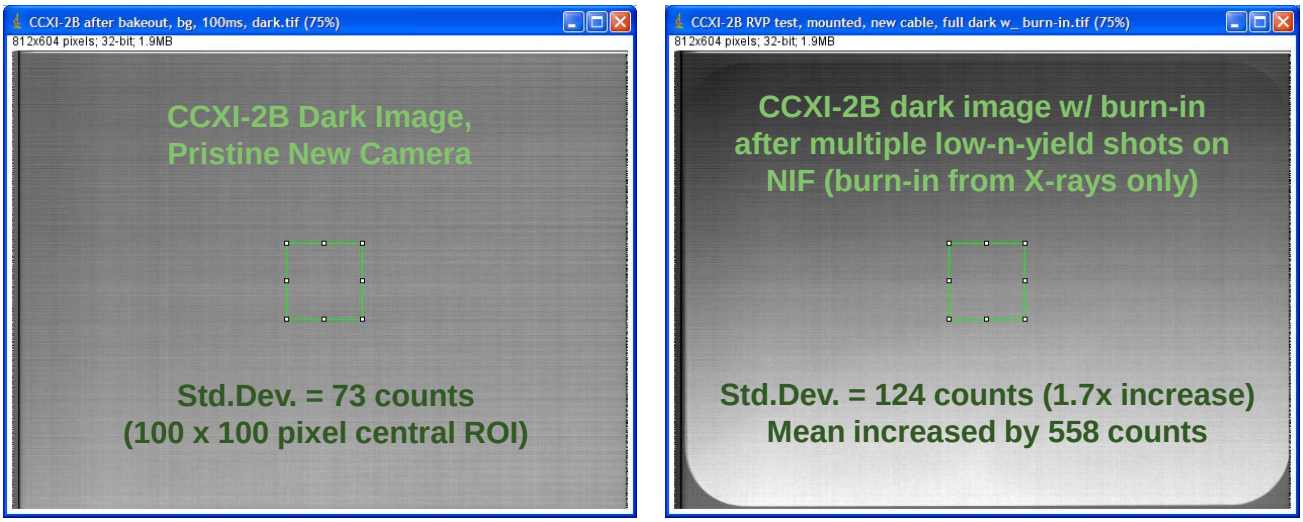

Figure 11. CID camera dark images before and after multiple X-ray exposures at NIF, showing the effect of X-ray damage. X-ray damage increases the pixel dark current, thereby decreasing the dynamic range.

5.4 Neutron damage

CCXI was tested for neutron damage on a series of high-yield shots listed in Table 2. The cumulative DT neutron fluence at the CID cameras for these shots was ~ 4.2×10^9 n/cm^2. The CCXI images for all these shots were highly saturated, and the cameras experienced upsets, producing shifted or incomplete images. However in subsequent dry-run images after each shot, the cameras operated normally again and the dark images had no measurable increase in dark current or noise. Said another way, any increase in noise due to neutron damage was much smaller than the existing sources of noise in our system, and could not be measured.

Table 2. Series of high-neutron-yield shots with CCXI-1 at 125 cm from the target.

Shot ID	DT n Yield, 14 MeV	DT Neutron Fluence* at CCXI (n/cm^2)
N110608	1.93×10^{14}	9.8×10^8
N110826	1.72×10^{14}	8.8×10^8
N110904	4.50×10^{14}	2.3×10^9

* Includes primary DT neutron fluence only. Total fluence including scattered neutrons was higher than this.

For illustration, a dark image taken after the last shot in Table 2 is shown in Figure 12. X-ray damage is evident from the burned-in pattern of the tungsten frame around the edge of the sensor, but there is no measurable damage due to neutrons.

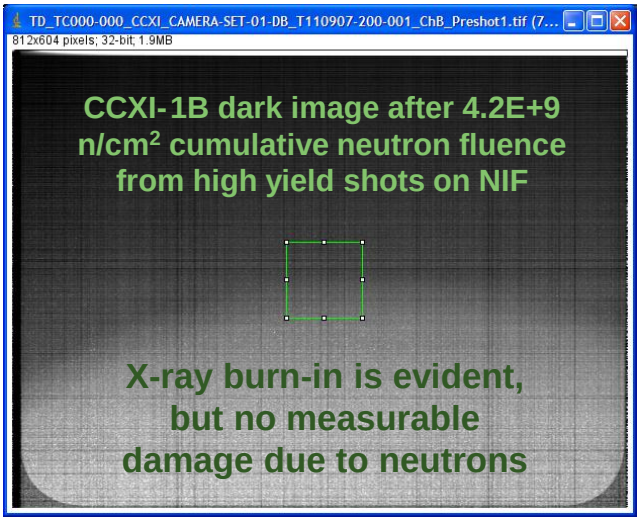

Figure 12. CID camera dark image after running on multiple high-neutron-yield shots at NIF.

6. CONCLUSIONS AND FUTURE WORK

The CID Camera X-ray Imager system has been designed, built, calibrated, and fielded at NIF on DIM-based diagnostics (GXD and hGXI) in DIM 0-0 and in DIM 90-78. (CCXI was not commissioned in DIM 90-315 due to shorts in the infrastructure cable.) The CID cameras were calibrated using X-ray sources at NSTec. The responsivity of the cameras was measured for X-rays from 3 – 14 keV. The camera resolution with 4.6 keV X-ray illumination was found to be ≈ 10 LP/mm. The CID camera linearity and saturation limits were also characterized using a visible light source. The CID cameras are suitable for various X-ray imaging applications at NIF.

CCXI performance and radiation hardness have been evaluated on shots at NIF in a harsh neutron environment. CCXI can acquire usable images for neutron fluence up to ~ 10^8 n/cm^2 (shot yield of ~ 5×10^{13} neutrons with the CIDs at 125 cm from the target). CCXI images saturated at higher neutron fluence, but the CID cameras survived with no measurable damage due to neutrons. (Two CID cameras were tested up to ~ 4.2×10^9 n/cm^2 cumulative DT neutron fluence.)

Recommendations for future work include upgrading the cable plant to transmit the clock and trigger signals via coax. instead of differential line pair, thereby reducing noise coupling into the readout; further improving the EMI shielding for CCXI; and fine-tuning the delay of the clock signal to get optimal analog-to-digital samples where noise in the readout waveform is lowest. Finally, CID cameras could be adapted for other time-integrated imaging applications at NIF such as EHXI (Equatorial Hard X-ray Imager) to replace image plates and attain the benefits of electronic data readout.

ACKNOWLEDGMENTS

The authors would like to thank Niko Izumi of LLNL for his calculation of the estimated saturation levels for these CID cameras compared to image plate, and Frederic Marshall of the Univ. of Rochester for sharing many valuable insights from his experience using these CID cameras at OMEGA.

This work was performed under the auspices of the U.S. Department of Energy by Lawrence Livermore National Laboratory under contract DE-AC52-07NA27344. Lawrence Livermore National Security, LLC. LLNL-CONF-XXXXXX

REFERENCES

[1] Carbone, J., et al., "Large format CID x-ray image sensor," Proc. SPIE 3301, 90-99 (1998).
[2] Carbone, J., et al., "Megarad and scientific CIDs," Proc. SPIE 2654, 131-138 (1996).
[3] Wentink, R. F., et al., "Charge injection device detectors for X-ray imaging," Proc. SPIE 2279, 380-387 (1994).
[4] Marshall, F. J., DeHaas, T., and Glebov, V. Y., "Charge-injection-device performance in the high-energy-neutron environment of laser-fusion experiments," Rev. Sci. Instrum. 81, 10E503 (2010).
[5] Marshall, F. J., et al., "Imaging of laser–plasma x-ray emission with charge-injection devices," Rev. Sci. Instrum. 72(1), 713-716 (2001).
[6] Oertel, J. A., et al., "Gated x-ray detector for the National Ignition Facility," Rev. Sci. Instrum. 77, 10E308 (2006).
[7] Opachich, Y. P., et al., "High performance imaging streak camera for the National Ignition Facility," Rev. Sci. Instrum. 83, 125105 (2012).
[8] Kyrala, G. A., et al., "Measuring symmetry of implosions in cryogenic Hohlraums at the NIF using gated x-ray detectors," Rev. Sci. Instrum. 81, 10E316 (2010).
[9] Thermo Scientific, CIDTEC Cameras & Imagers, 101 Commerce Blvd., Liverpool, NY 13088. http://www.thermoscientific.com/CIDTEC
[10] CIDTEC Cameras and Imagers Radiation hardened camera product line, (Accessed 1 September 2013), http://www.thermoscientific.com/ecomm/servlet/techresource?resourceId=81580&storeId=11152&from=search#
[11] Jupiter Laser Facility at Lawrence Livermore National Laboratory, https://jlf.llnl.gov/
[12] Haugh, M. J., et al., "Calibration of X-ray imaging devices for accurate intensity measurement," Powder Diffr. 27(2), 79-86 (2012).
[13] Janesick, J., [Photon Transfer DN → λ], SPIE Press, Bellingham, Washington, 68, (2007).